1832
doi:10.1017/S1431927618009649
Microsc. Microanal. 24 (Suppl 1), 2018


# *In situ* Single/Cyclic Deformation and Correlated Precession Electron Diffraction Analysis of Nano-laminate Crystalline/Glassy Metal Composites

Qianying Guo[1], Christopher M. Barr[2], Khalid Hattar[2] and Gregory B. Thompson[1]

[1.] The University of Alabama, Department of Metallurgical & Materials Engineering, Tuscaloosa, AL, USA.
[2.] Sandia National Laboratories, Department of Radiation Solid Interactions, Albuquerque, NM, USA.

Amorphous materials have been shown to exhibit unique mechanical behavior including high yield strengths and elastic limits, but they suffer limited fracture plasticity [1, 2]. By introducing a crystalline phase into the amorphous material, this catastrophic fracture failure within the glassy phase can be mitigated [2]. Recognizing that dislocation-based plasticity occurs within the crystalline phase and shear banding within the glassy phase, understanding this co-deformation, particularly at the crystalline/amorphous interface, is an area for fertile research investigation. In this paper, a nano-laminate structure was fabricated to precisely control the volume fraction and length scale of the crystalline phase within the glassy matrix. Using an *in situ* transmission electron microscopy (TEM) single/cyclic deformation holder with correlative precession electron diffraction (PED), the microstructure evolution during deformation in these nanoscale composites was quantified [3, 4].

A series of amorphous $Cu_{45}Zr_{55}$ (at. %, 3 layers)/crystalline Cu (2 layers) nano-laminates were sputter-deposited onto Si wedges. The thickness of the glassy layers was maintained at 150 nm with varying Cu layer thicknesses from 20 nm to 100 nm. To create a continuous, electron transparent foil from the film to the substrate on the wedge, focus ion beam milling was employed following a thinning procedure in reference [5]. The thin foils were then deformed by a cube corner diamond tip inside the (TEM). Real-time load-displacement values, Fig. 1(a) and Fig. 2(a), as well as the corresponding bright field images, Fig 1(b)-(d) and Fig. 2(b)-(d), were recorded during the mechanical tests. In the bright field images, the dynamical contrast (as well as other forms of contrast) created under deformation can mask features of interest from easy viewing. Using PED, the grain sizes and grain boundaries can be easily viewed, even if the bright field image does not clearly reveal these microstructural features. Thus, by combining the PED technique with *in situ* deformation, the quantitative effects of both loading condition and intrinsic microstructure evolution can now easily be linked.

For the nanoindentation test on the $Cu_{45}Zr_{55}$ (150 nm)/crystalline Cu (100 nm) laminate, 3 loading conditions were selected on the load-displacement curve in Fig. 1(a). According to Fig. 1(b) to (d), grain growth and grain rotation was observed in the corresponding bright field images and further confirmed by the inserted inverse pole figure maps from PED. A previous large grain in region 1 became even larger after indentation, indicating a sliding movement of the surrounding grains [6]. In addition, some orientation changes of the grains were also noted in region 2, comparing to their neighbouring grains. An increasing contrast is observed in the amorphous layer near the indent, indicating a possible strain induced density enhancement of the glassy phase. For the cyclic deformation test, a two-step 20 Hz cyclic loading on the same sample was performed and the load-time curve is shown in Fig. 2(a). Correlated microstructure analysis of pre-fatigue (0 cycle), post-1st fatigue (8,000 cycles), and post-2nd fatigue (28,000 cycles) are presented in Fig. 2(b)-(d). A relatively lower cyclic loading amplitude with limited cycles indicates it will induce a rearrangement of the nanocrystalline Cu grain, Fig. 2(c). While increasing load and cycles, the rearranged small grains began to coalesce and form several large grains, with or

without orientation changes, Fig. 2(d). In addition, limited contrast changes were observed in the amorphous layer under the indenter compared to that of single indentation. The detail links of how microstructure changes with the loading conditions and the Cu layer thickness will be discussed using this *in situ* deformation and cross-correlated PED technique [7].

References:

[1] Greer, A. *et al*, Materials science and Engineering: R: Report **74** (2013), p. 71-132.
[2] Schuh, C. *et al*, Acta Materialia **55** (2007), p. 4067-4109.
[3] Bufford, D. *et al*, Nano Letters **16** (2016), p. 4946-4953.
[4] Kobler, A. *et al*, Ultramicroscopy **128** (2013), p. 68-81.
[5] Giannuzzi, L. *et al*, Micron **30** (1999), p. 197-204.
[6] Van Swygenhoven, H. *et al*, Physical Review B **64** (2001), p. 224105.
[7] The authors gratefully recognize support from the ARO W911NF-17-1-0528. This work was performed, in part, at the Center for Integrated Nanotechnologies, an Office of Science User Facility operated for the U.S. Department of Energy (DOE) Office of Science. Sandia National Laboratories is a multi-mission laboratory managed and operated by National Technology and Engineering Solutions of Sandia, LLC, a wholly owned subsidiary of Honeywell International, Inc., for the U.S. Department of Energy's National Nuclear Security Administration under contract DE-NA-0003525. The Bruker PI-95 indenter was acquired through the NSF-DMR-1531722.

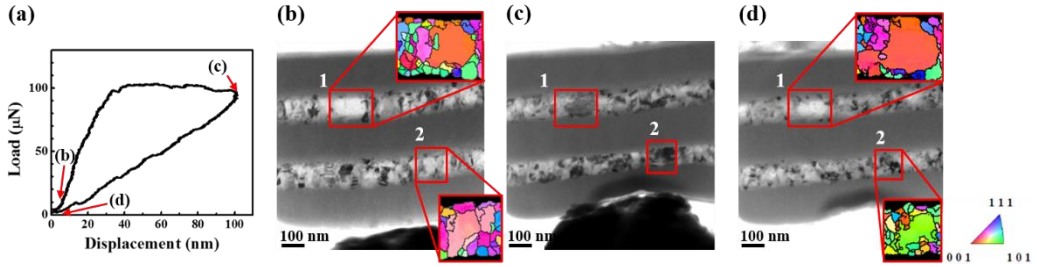


**Figure 1.** **(a)** Single load-displacement curve of nanoindentation test of the $Cu_{45}Zr_{55}$/Cu nanolaminate. Three-points are selected on the curve with corresponding TEM bright field images shown from (b) to (d). **(b)** TEM bright field image at point (b) pre-deformation. Two region of interests (ROIs) are selected with the magnified IPF maps inserted. **(c)** TEM bright field image at point (c) under maximum displacement (100 nm) with contrast changes in the ROIs. **(d)** TEM bright field image at point (d) post-deformation. The magnified IPF maps of the ROIs are inserted, showing grain growth and grain rotation.

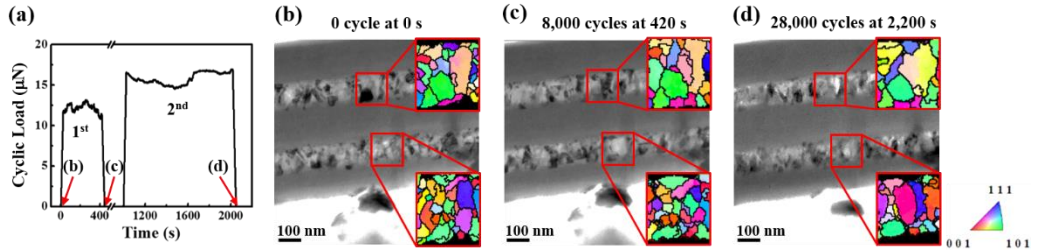


**Figure 2.** **(a)** Cyclic load-time curve of fatigue test of the $Cu_{45}Zr_{55}$/Cu nanolaminate. Three-points are selected on the curve with corresponding TEM bright field images shown from **(b)** to **(d)**. **(b)** TEM bright field image at point (b) under 0 cycle. Two region of interests (ROIs) are selected with the magnified IPF maps inserted. **(c)** TEM bright field image at point (c) under 8,000 cycles. The magnified IPF maps of the ROIs are inserted, showing grain rearrangement. **(d)** TEM bright field image at point (d) under 28,000 cycles. The magnified IPF maps of the ROIs are inserted, showing grain growth.

https://doi.org/10.1017/S1431927618009649 Published online by Cambridge University Press